Structure, morphology and composition of natural junctions of Sr_2RuO_4–$Sr_3Ru_2O_7$ eutectic crystals

2009 J. Phys.: Condens. Matter 21 254211

(http://iopscience.iop.org/0953-8984/21/25/254211)

J. Phys.: Condens. Matter **21** (2009) 254211 (5pp) doi:10.1088/0953-8984/21/25/254211

Structure, morphology and composition of natural junctions of Sr_2RuO_4–$Sr_3Ru_2O_7$ eutectic crystals

R Fittipaldi[1,2], **Y Maeno**[3] **and A Vecchione**[1,2]

[1] CNR-INFM Laboratorio Regionale SuperMat Salerno, via S Allende 84081 Baronissi(Sa), Italy
[2] Dipartimento di Fisica E.R. Caianiello, Universitá di Salerno, via S. Allende 84081 Baronissi(Sa), Italy
[3] Department of Physics, Graduate School of Science, Kyoto University, Kyoto 606-8502, Japan

E-mail: vecchione@sa.infn.it

Received 24 March 2009
Published 29 May 2009
Online at stacks.iop.org/JPhysCM/21/254211

Abstract
A detailed study of morphological, compositional and structural aspects of Sr_2RuO_4–$Sr_3Ru_2O_7$ eutectic crystals is reported. The stoichiometry of the phases that compose the crystals and how they are arranged in the crystals are studied. Understanding the behavior at the Sr_2RuO_4–$Sr_3Ru_2O_7$ interface represents a necessary prerequisite for the analysis of the experimental results on the transport properties recently reported in the literature.

(Some figures in this article are in colour only in the electronic version)

1. Introduction

Layered strontium ruthenates are currently a subject of intense investigation due to many fascinating properties [1–4]. Recently, superconducting behavior in Sr_2RuO_4–$Sr_3Ru_2O_7$ eutectic crystals has been observed [5–7]. In particular, an experimental study on the critical current in the $Sr_3Ru_2O_7$ region of the eutectic crystal has been carried out at different distances from the interface between the triplet superconductor (Sr_2RuO_4) and the metamagnetic compound ($Sr_3Ru_2O_7$) [8]. The critical current was measured deep in the $Sr_3Ru_2O_7$ area at distances of millimeters from the interface with the Sr_2RuO_4 region. One can understand the unusual superconducting behavior experimentally detected asserting the presence of Sr_2RuO_4 inclusions in the $Sr_3Ru_2O_7$ region or drawing the outline of various possible exotic scenarios [6–8]. To explore these systems where unconventional superconductivity and collective magnetic behavior can be matched at the nanoscale, it is very important to view the interface quality of the junctions involved.

In this work, we perform a detailed investigation of the morphological, compositional and structural aspects of Sr_2RuO_4–$Sr_3Ru_2O_7$ eutectic crystals. The present study is particularly addressed to the understanding of how the phases are arranged in the eutectic crystals and how they match each other.

2. Microstructure of the crystals

The synthesis of Sr_2RuO_4–$Sr_3Ru_2O_7$ eutectic crystals by a flux-feeding floating zone technique has been previously reported [5]. In brief, this growth technique consists of melting the bottom end of a feed rod suspended from above and connecting the molten zone to a seed held from below. A single crystal is continuously grown from the molten solution by moving both the seed material and the feed rod through the hot molten zone. The crystals grown by this technique have the advantage of low impurity content, high homogeneity and large size. Similarly to pure Sr_2RuO_4 crystals, the Sr_2RuO_4–$Sr_3Ru_2O_7$ samples can be easily cleaved along the a–b plane. For a morphological investigation the first step was to look at the crystals by polarized light optical microscopy (PLOM). Because of the different refractive indices of the two phases, we observed two different regions. As we will show in the following through compositional analysis, the bright areas of the sample are the $Sr_3Ru_2O_7$ phase while the dark ones are Sr_2RuO_4. The PLOM investigation was performed on the cleaved surface (a–b plane) and on surfaces cut perpendicularly (a–c and b–c planes) to the cleaving plane.

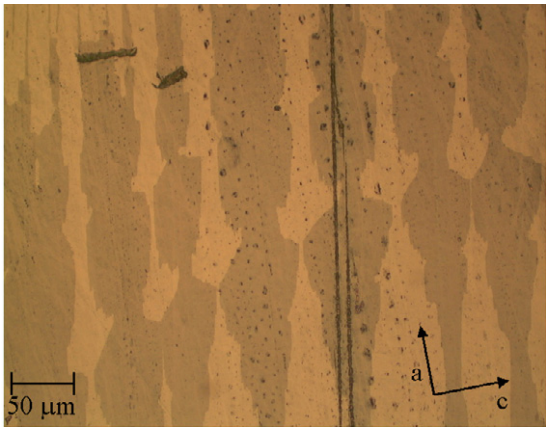

Figure 1. Polarized light optical microscopy image of polished *a–c* plane of a sample showing oscillations in the lamellar pattern.

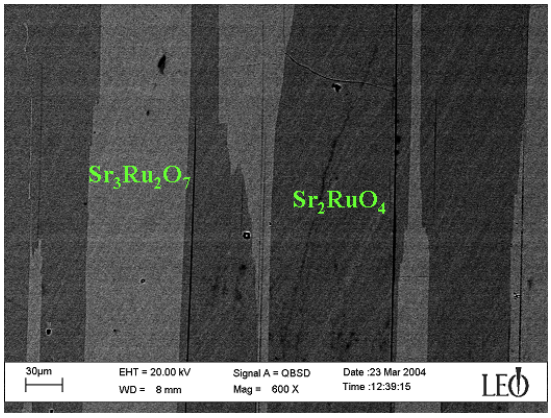

Figure 2. BSE image of the eutectic crystal showing the contrast related to the different atomic number ratios Sr/Ru of the compounds constituting the two phases. The bright areas are $Sr_3Ru_2O_7$ while dark ones are Sr_2RuO_4.

As a consequence of different growth conditions the PLOM images of many crystals along the *a–c* plane showed eutectic, hypo-eutectic and hyper-eutectic solidification [9].

In figure 1 a PLOM image of the *a–c* plane is given for a crystal showing a regular lamellar structure of Sr_2RuO_4 and $Sr_3Ru_2O_7$, typical of solidification passed near the eutectic point. The order of magnitude of the lamellar spacing, equal to tens of microns, is in agreement with the values already reported for other eutectic crystals [10]. By studying the morphologies of the lamellae it is evident that they depend sensitively on details of the growth conditions, especially on whether or not steady growth of the crystal was obtained [11]. In addition, in the case of a lamellar eutectic growth, the lamellar spacing (λ) fundamentally depends on the solid–liquid interface undercooling. Jackson and Hunt [12] first analyzed eutectic solidification, assuming steady state at a constant growth velocity of the eutectic mixture, V_f, and predicted that $\lambda^2 V_f$ should be constant, in agreement with some experiments [13, 14]. Moreover, in practice most eutectic systems tend to solidify for V_f in the μm s^{-1} range and with interlamellar spacing typically of the order of few μm, so laboratory samples contain hundreds of lamellae. In our case, Sr_2RuO_4–$Sr_3Ru_2O_7$ eutectic crystals solidified for a V_f of about 4.2 μm s^{-1}, and measuring the period of the lamellar pattern on different crystals and in different areas of the same crystal, we obtained a lamellar period ranging from 20 to 130 μm. The spread of the lamellar spacing over a large range of values is not unusual and has also been observed in other eutectic systems [15, 16]. Looking over the lamellar pattern (see figure 1) a slight oscillation of the lamellar patterns is observable. The appearance of regular oscillations in eutectic lamellar solidification was experimentally observed and theoretically predicted as related to the breakdown of the steady state lamellar eutectic structure.

In other cases the lamellae were found to be very regularly arranged. By cutting the crystals perpendicularly to the lamellar direction (*b–c* plane) we observed that the lamellae were three dimensional, parallel to each other in *a–b* planes and oriented along the growth direction to form a sort of microsized stacking of natural multi-layers piled up along the *c* axis.

In order to determine their qualitative composition and the possible secondary phases, the crystals were analyzed using a LEO-EVO 50 scanning electron microscope (SEM). In particular, back-scattered electron (BSE) images confirmed the presence of only two phases. Figure 2 shows an example of a BSE image taken from a polished crystal showing a lamellar pattern (*a–c* plane). The bright lamellae had the composition of $Sr_3Ru_2O_7$ phase while the dark ones were Sr_2RuO_4 phase as we will see in section 3. At this level, BSE images showed the absence of spurious phases within each lamella and no evidence of Sr_2RuO_4 lamellae finely incorporated into the $Sr_3Ru_2O_7$ ones and vice versa.

3. Compositional analysis

An energy dispersive spectrometer (EDS, Oxford INCA Energy 300) and a wavelength dispersive spectrometer (WDS, Oxford INCA Wave 700) were used for overall microstructural and compositional analysis of the samples.

In the EDS method, data collection and analysis are processed from a spectrum of energies acquired simultaneously. Using WDS, the spectrum is acquired sequentially as the full wavelength range is scanned. Although it takes longer to acquire a full spectrum, the WDS technique has led to a significant improvement of the resolution and the sensitivity compared to EDS.

In our study we used both of the microanalysis techniques. EDS was used routinely for the survey of the samples, while the resolution and dynamic range of WDS were employed to check for the overlaps and increased sensitivity for trace elements. The available detectors can provide information starting from elements with $Z \geqslant 4$. EDS and WDS analysis were performed by operating at 20 keV primary energy with a probe current of 100 pA for the former and at 20 keV primary energy and probe current of 5 nA for the latter. The composition of each measured crystal was derived by averaging all EDS data acquired over different areas, normalizing them such that Sr = 2 or 3. The results for selected samples are reported in table 1.

Table 1. Summary of compositional results obtained by EDS analysis. The phases identified are Sr_2RuO_4 and $Sr_3Ru_2O_7$.

Sample	Phase 1	Phase 2
cfv08	$Sr_2Ru_{1.08}O_{4.75}$	$Sr_3Ru_{2.06}O_{7.93}$
cfv07	$Sr_2Ru_{0.98}O_{4.43}$	$Sr_3Ru_{1.96}O_{7.71}$
cfv12	$Sr_2Ru_{1.00}O_{4.31}$	$Sr_3Ru_{1.97}O_{7.46}$

Table 2. Summary of compositional results obtained by WDS analysis. The phases identified are Sr_2RuO_4 and $Sr_3Ru_2O_7$.

Sample	Phase 1	Phase 2
cfv07	$Sr_2Ru_{1.06}O_{4.04}$	$Sr_3Ru_{2.09}O_{6.70}$
cfv12	$Sr_2Ru_{1.06}O_{4.02}$	$Sr_3Ru_{2.08}O_{7.03}$

The data show that only two phases identified with Sr_2RuO_4 and $Sr_3Ru_2O_7$ were present in the samples. This result was confirmed by WDS analysis. Data summarized in table 2 represent the mean value over many WDS acquisitions for each phase. By comparing the compositional analysis extracted from by the two techniques, good agreement is evident.

This analysis indicated that each phase was homogeneous in the Sr/Ru atomic ratio. To understand how the composition changed by moving from one phase to the other EDS analysis was performed along a line crossing the interface between two adjacent lamellae. Recalling that the lateral resolution of the EDS technique is about 1 μm, we chose to carry out the acquisitions with beam points separated from each other by only by a few μm. In table 3 some of the results obtained are summarized. The X and Y coordinates reported in table 3 represent the electron beam position; the Y coordinate is along a direction of the lamellae. In these measurements Y was kept constant during the X scan. As one can observe from table 3, we moved from an area with composition $Sr_3Ru_2O_7$ to one with Sr_2RuO_4 stoichiometry. The changes in composition crossing the interface were sharp as is seen from spectrum 5 to spectrum 6 in table 3.

EDS analysis was also performed along the direction of the lamellae profile. An example of this kind of measurement is summarized in table 4. In this case, the analysis revealed a composition of Sr_2RuO_4 along the interface. Here, the X and Y coordinates both change to follow the path of the lamellae. Using WDS techniques, a range of wavelengths between 2.48 and 23.79 Å was scanned to check traces of different elements. Scans of approximately 10 h/sample were performed to check the presence of elements with Z ranging from 5 (B) to 83 (Bi). In figure 3, where a scan over a part of the wavelength range taken from sample cfv12 is shown, all the visible major peaks are attributable to reflections from x-rays characteristic of Sr or Ru. Our investigations showed in the $Sr_3Ru_2O_7$ domain of the eutectic crystals traces of Al and Si less than 50 ppm. The same analysis on the Sr_2RuO_4 domain (figure 3) did not show any spurious elements.

4. Crystal structure and orientation

We determined the crystal structure and the lattice parameters at room temperature for pure Sr_2RuO_4 and $Sr_3Ru_2O_7$ single crystals, and for Sr_2RuO_4–$Sr_3Ru_2O_7$ eutectic crystals by means of x-ray diffraction. A Philips X'Pert-MRD high-resolution analytic diffractometer equipped with a four-circle cradle was used. A Cu Kα_1 ($\lambda = 1.5406$ Å) source was used at 40 kV and 40 mA. The angles ω and 2θ were used according to the standard definition in x-ray diffraction.

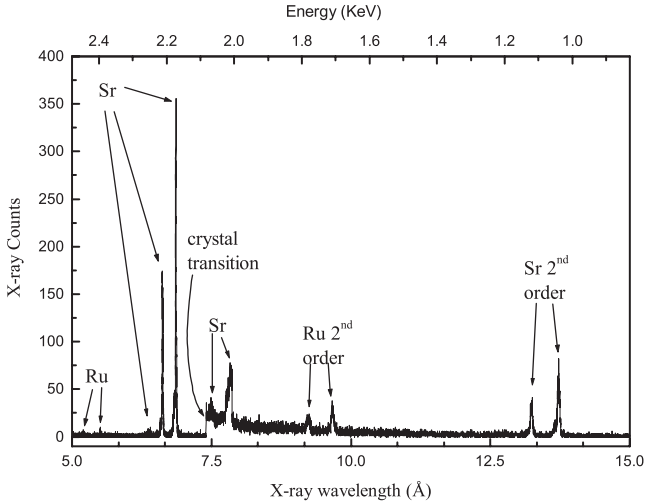

Figure 3. WDS trace element scans in the wavelength range 5–15 Å for the Sr_2RuO_4–$Sr_3Ru_2O_7$ eutectic crystal. All the visible peaks are first or higher order Bragg reflections of x-rays characteristic of Sr or Ru.

To check the crystallographic orientation of the two phases in our eutectic crystal we carried out 2θ–ω scans of the polished surface cleaved from the crystals. These measurements were made on a number of cleaved surfaces of eutectic crystals taken from different portions of each sample. The XRD pattern taken on this surface (not shown here) is consistent with the presence of only two phases in agreement with the compositional analysis. All the diffraction peaks can be identified with the expected (0 0 l) Bragg reflections coming from Sr_2RuO_4 and $Sr_3Ru_2O_7$. 2θ–ω measurements on crushed crystal also supported this result. The FWHM $= 0.02°$ of the detected peaks is comparable with the one measured on pure Sr_2RuO_4 crystals, pointing out a strong compositional homogeneity.

To show possible misalignments between c-axes of Sr_2RuO_4 and $Sr_3Ru_2O_7$ phases and imperfect crystalline layered structures, we carried out reciprocal space mapping (RSM). Characterization of Sr_2RuO_4 and $Sr_3Ru_2O_7$ domain structures in our eutectic crystals was carried out by studying the ω–$2\theta/\omega$ diffraction space mapping around Sr_2RuO_4(0 0 12) and $Sr_3Ru_2O_7$(0 0 20) reflections.

As an example, in figure 4 the ω–$2\theta/\omega$ mapping of Sr_2RuO_4(0 0 12) and $Sr_3Ru_2O_7$(0 0 20) is reported.

The points in the x-ray diffraction maps have shapes which depend upon the sample dimensions and perfection. The measurements in figure 4 point out a large broadening in the ω direction for the reflections of both phases. By comparing (figure 5) the x-ray diffraction maps for the (0 0 12) Bragg reflection of the pure Sr_2RuO_4 crystal, the presence of very small broadening in ω is evident, demonstrating an excellent crystallinity in this case. Similar ω–$2\theta/\omega$ maps (not reported

Table 3. Results of EDS compositional analysis performed across the interface between two lamellae. X and Y are the beam position. The results are shown as atomic percentages.

Spectrum	X (μm)	Y (μm)	O (at.%)	Sr (at.%)	Ru (at.%)	Composition
1	−7.934	−10.098	58.99	24.88	16.13	$Sr_3Ru_{1.94}O_{7.11}$
2	−6.331	−10.098	60.02	24.62	15.37	$Sr_3Ru_{1.87}O_{7.31}$
3	−4.729	−10.098	59.04	24.73	16.23	$Sr_3Ru_{1.97}O_{7.16}$
4	−3.046	−10.098	59.62	24.53	15.85	$Sr_3Ru_{1.94}O_{7.29}$
5	−1.443	−10.098	59.46	24.68	15.86	$Sr_3Ru_{1.93}O_{7.23}$
6	0.160	−10.098	57.93	27.95	14.12	$Sr_2Ru_{1.01}O_{4.15}$
7	1.763	−10.098	58.93	27.64	13.43	$Sr_2Ru_{0.97}O_{4.26}$
8	3.366	−10.098	58.78	27.58	13.65	$Sr_2Ru_{0.99}O_{4.26}$
9	5.049	−10.098	58.74	27.33	13.93	$Sr_2Ru_{1.02}O_{4.30}$
10	6.652	−10.098	58.21	28.11	13.67	$Sr_2Ru_{0.97}O_{4.14}$

Table 4. Results of EDS compositional analysis performed along the interface. X and Y are the beam position. The results are shown as atomic percentages.

Spectrum	X (μm)	Y (μm)	O (at.%)	Sr (at.%)	Ru (at.%)	Composition
1	−13.885	42.698	58.63	27.74	13.64	$Sr_2Ru_{0.98}O_{4.23}$
2	−13.538	37.838	58.39	27.76	13.84	$Sr_2Ru_{1.00}O_{4.21}$
3	−13.191	16.547	58.38	28.04	13.58	$Sr_2Ru_{0.97}O_{4.16}$
4	−12.034	4.628	58.60	27.64	13.76	$Sr_2Ru_{1.00}O_{4.24}$
5	−12.034	−6.017	59.13	27.20	13.67	$Sr_2Ru_{1.01}O_{4.35}$
6	−14.464	−30.085	58.82	27.58	13.60	$Sr_2Ru_{0.99}O_{4.27}$
7	−11.687	−18.167	57.97	28.21	13.81	$Sr_2Ru_{0.98}O_{4.11}$
8	−14.464	−33.441	58.51	27.70	13.79	$Sr_2Ru_{1.00}O_{4.22}$
9	−13.885	−22.448	57.95	28.34	13.71	$Sr_2Ru_{0.97}O_{4.09}$
10	−13.885	−22.217	59.00	27.38	13.62	$Sr_2Ru_{0.99}O_{4.31}$

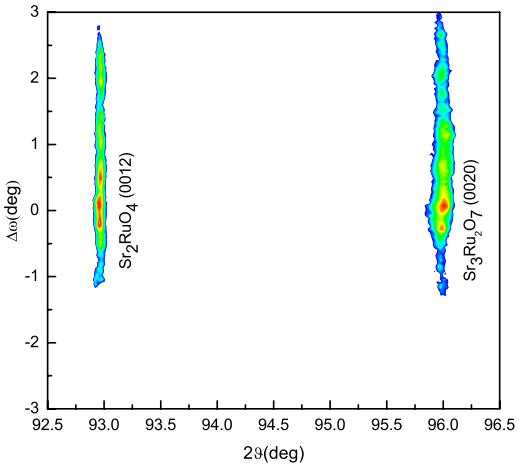

Figure 4. ω–$2\theta/\omega$ maps of Sr_2RuO_4(0 0 12) and $Sr_3Ru_2O_7$(0 0 20) reflections. The positions of the points show c-axis alignment of the two phases. The points of the x-ray diffraction map have a large broadening in ω.

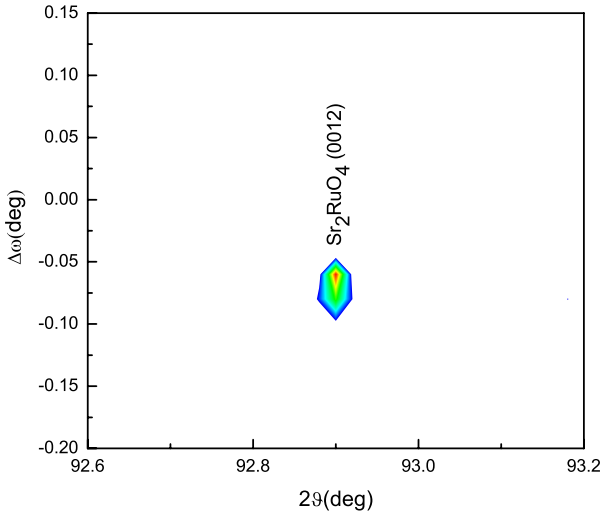

Figure 5. ω–$2\theta/\omega$ maps of the Sr_2RuO_4(0 0 12) reflection; a very small broadening in ω is evident in agreement with the excellent crystallinity shown by the rocking curve.

here) were also measured in pure $Sr_3Ru_2O_7$ single crystals. More detailed rocking curves (ω-scans) acquired for eutectic crystals and pure Sr_2RuO_4 crystals also support the strong differences in the two kinds of samples, the FWHM being equal to 3° and 0.03°, respectively.

The broadening in ω observed in the eutectic crystals can be interpreted as due to mosaic spread of the many Sr_2RuO_4–$Sr_3Ru_2O_7$ interfaces contributing to the measure. Because the lamellar patterns of the eutectic crystals were not regular (also with oscillations as seen before), the resulting interfaces are wavy. This aspect is relevant whenever this kind of natural junctions is employed in experiments devoted to the study of the transport properties of these materials.

References

[1] Maeno Y, Hashimoto H, Yoshida K, Nishizaki S, Fujita T, Bednorz J G and Lichtenberg F 1994 *Nature* **372** 532
[2] Mackenzie A P and Maeno Y 2003 *Rev. Mod. Phys.* **75** 657
[3] Grigera S A, Gegenwart P, Borzi R A, Weickert F, Schofield A J, Perry R S, Tayama T, Sakakibara T, Maen Y, Green A G and Mackenzie A P 2004 *Science* **306** 1154

[4] Borzi R A, Grigera S A, Farrell J, Perry R S, Lister S J S, Lee S L, Tennant D A, Maeno Y and Mackenzie A P 2007 *Science* **315** 214
[5] Fittipaldi R, Vecchione A, Fusanobori S, Takizawa T, Yaguchi H, Hooper J, Perry R S and Maeno Y 2005 *J. Cryst. Growth* **282** 152
[6] Hooper J, Zhou M, Mao Z Q, Liu Y, Perry R S and Maeno Y 2006 *Phys. Rev.* B **73** 132510
[7] Kittaka S, Fusanobori S, Yaguchi H, Maeno Y, Fittipaldi R and Vecchione A 2008 *Phys. Rev.* B **77** 214511
[8] Fittipaldi R, Vecchione A, Ciancio R, Pace S, Cuoco M, Stornaiuolo D, Born D, Tafuri F, Olsson E, Kittaka S, Yaguchi H and Maeno Y 2008 *Europhys. Lett.* **83** 27007
[9] Fittipaldi R, Fusanobori S, Kittaka S, Yaguchi H, Hooper J, Vecchione A and Maeno Y 2007 *Physica* C **460–462** 524
[10] Okane T and Umeda T 1998 *ISIJ Int.* **38** 454
[11] Lan C W 2003 *J. Cryst. Growth* **247** 597
[12] Jackson K A and Hunt J D 1966 *Trans. Met. Soc. AIME* **236** 1129
[13] Zimmerman M, Karma A and Carrard M 1990 *Phys. Rev.* B **42** 833
[14] Caroli C and Faivre G 1995 *Key Eng. Mater.* **103** 1
[15] Aguiar M R and Caram R 1997 *J. Cryst. Growth* **174** 70
[16] Fittipaldi R, Sisti D, Vecchione A and Pace S 2007 *Cryst. Growth Des.* **7** 2495